



# A gradient-boosted tree framework to model the ice thickness of the World's glaciers (IceBoost v1)

Niccolò Maffezzoli<sup>1,2,3</sup>, Eric Rignot<sup>2,4</sup>, Carlo Barbante<sup>1,2</sup>, Troels Petersen<sup>5</sup>, and Sebastiano Vascon<sup>1</sup>

<sup>1</sup>Ca' Foscari University of Venice, Venezia, Italy

<sup>2</sup>University of California Irvine, Irvine, USA

<sup>3</sup>Institute of Polar Sciences, National Research Council, Venezia, Italy

<sup>4</sup>Jet Propulsion Laboratory, Pasadena, USA

<sup>5</sup>Niels Bohr Institute, University of Copenhagen, Copenhagen, Denmark

**Correspondence:** Niccolò Maffezzoli (niccolo.maffezzoli@unive.it)

**Abstract.** Knowledge of glacier ice volumes is crucial for constraining future sea level potential, evaluating freshwater resources, and assessing impacts on societies, from regional to global. Motivated by the disparity in existing ice volume estimates, we present IceBoost, a global Machine Learning framework to model individual glacier ice thickness distributions. IceBoost is an ensemble of two gradient-boosted trees trained with 3.7 million globally-available ice thickness measurements and an array of 34 numerical features. The model error is similar to existing models outside polar regions and up to 30-40% lower at high latitudes. Providing supervision by exposing the model to available glacier thickness measurements reduces the error by up to a factor 2 to 3. A feature ranking analysis reveals that geodetic information are the most informative variables, while ice velocity can improve the model performance by 6% at high latitudes. A major feature of IceBoost is a capability to generalize outside the training domain, i.e. producing meaningful ice thickness distributions in all regions of the World, including in the ice sheet peripheries.

## 1 Introduction

Under atmospheric heating by human forcing, with few exceptions, glaciers have been retreating worldwide at unprecedented rates (Hugonnet et al., 2021), with projections predicting one third of the mass loss at the end of the century in the most optimal +1.5°C scenario (Rounce et al., 2023). At present, glacier melting contributes to sea level rise equally to ice sheets (Zemp et al., 2019; Masson-Delmotte et al., 2021), with far reaching implications for coastal communities worldwide (Pörtner et al., 2019). Ice mass loss from glacier shrinkage also impacts water availability for an estimated population of 1.9 billion people living in or depending on glacier-sourced freshwater (Huss and Hock, 2018; Rodell et al., 2018; Immerzeel et al., 2020).

Accurate and continuous knowledge of glacier ice thickness distributions over time is thus of critical importance to inform and refine numerical models to better simulate future scenarios under a fast-changing climate. Measurement campaigns and surveys have led to direct ice thickness measurements for about 3,000 of the existing more than 216,000 glaciers (Welty et al., 2020). The data is unsurprisingly sparse, albeit radar surveys from airborne campaigns have significantly increased the amount

of measurements and coverage, particularly over polar regions. Knowledge of absolute glacier volume thus heavily relies on models, or physical and mathematical interpolations.

An array of models has been proposed over time, with varying degrees of applicability (Farinotti et al., 2017). Only two exist for all glaciers on Earth. They are based on principles of ice flow dynamics and use surface characteristics, including ice surface velocity. The mass conservation approach by Huss and Farinotti (2012) has been extended with four additional regional models to produce a global consensus ensemble (Farinotti et al., 2019). More recently, Millan et al. (2022) also provided a global solution, leveraging a complete coverage of glacier velocities and using a shallow-ice approximation (Cuffey and Paterson, 2010).

Few approaches based solely on deep learning have been explored so far. Clarke et al. (2009) proposed a multilayer perceptron trained on neighboring deglaciated regions to reconstruct glacier bedrocks. Convolutional neural networks (CNN) are now the state-of-the-art architectures for physical models emulators, and they have gained traction in glaciology with Jouvét et al. (2022); Jouvét (2023). Trained to represent physical models with much cheaper computation cost, emulators have the versatility to both compute forward modeling and to invert for ice thickness. Uroz et al. (2024) trained a CNN to produce ice thickness maps on 1,400 Swiss glaciers, by ingesting surface velocity and Digital Elevation Model (DEM) maps, with their ground truth consisting of ice thickness fields obtained by a combination of experimental data and glaciological modeling. Growing attention is being directed to physics-informed neural networks, as they provide a natural setup to both generate an approximate solution of a differential equation and minimize the misfit with observational data, if any. For a review, we refer the readers to Liu et al. (2024).

In this work, we present IceBoost, a comprehensive, data-driven machine learning system designed for modeling ice thickness across all of Earth's glaciers, including continental glaciers, ice caps, and ice masses at the edges of ice sheets. We approach the problem as a machine learning regression task, predicting ice thickness at any point within a glacier's boundary. IceBoost employs an ensemble of two gradient-boosted decision tree models, XGBoost and CatBoost, which are trained using the Global Ice Thickness Database (GlaThiDa, or GTD hereafter), a centralized effort by the World Glacier Monitoring Service (WGMS) and detailed by Welty et al. (2020). We inform the model using a set of 34 numerical features, extracted from an array of products and organized in a tabular structure. While convolutional layers and deep learning are best suited for images in this context, when features are heterogeneous and arranged in a tabular structure, tree-based regressors often provide a much faster and more powerful alternative (Grinsztajn et al., 2022).

In the following sections we introduce the model concepts (Sect. 2), describe its interpretability (Sect. 3), illustrate the model inference on a global scale and compare its performance against existing global solutions (Sects. 4-4.1), consider the computational cost (Sect. 5), before we conclude (Sect. 6).

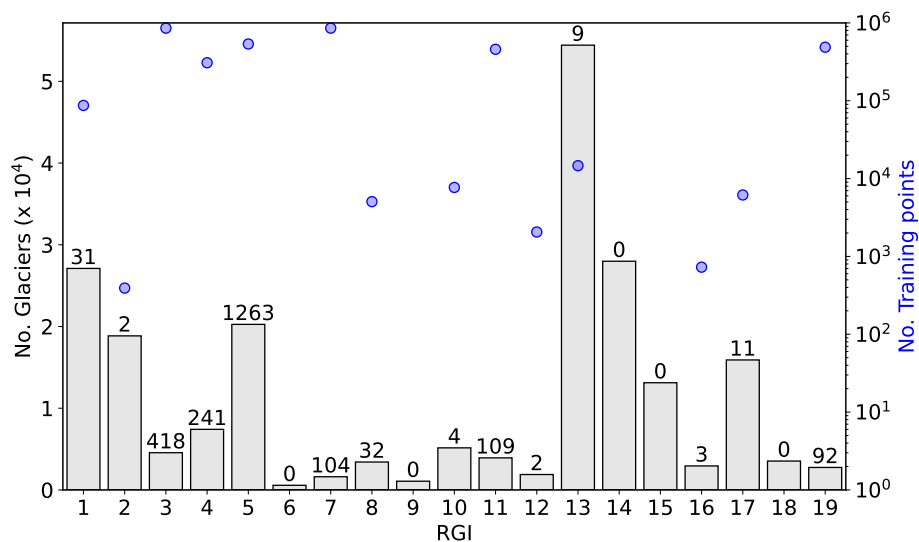


**Figure 1.** Statistics of glaciers and training data for each Randolph Glacier Inventory (RGI) region. The numbers on the bars represent the count of glaciers with training data. RGI 6, 9, 14 and 15 have no training data.

## 2 Methods

Hereafter, we describe the datasets used to produce the features needed to construct the training set, as well as to generate the model inputs at inference time. A more detailed description of the features, as well as the imputation policies, is provided in

55 Appendix A.

### 2.1 Dataset collection and training dataset

As ground truth, we use the GlaThiDa v. 3.1.0 dataset (GlaThiDa Consortium 2020; Welty et al. 2020), with 3.8 million ice thickness measurements. The features used to train the model are computed from various datasets and products (Table 1). Elevation and geodetic information are extracted or calculated from the global Tandem-X 30m Edited Digital Elevation Model (EDEM, Bueso-Bello et al. 2021; González et al. 2020; Martone et al. 2018). The DEM choice is determined by best trade-off between accuracy, resolution, and computational cost. Mass balance information is obtained from the Regional Atmospheric Climate Model (RACMO2) products at different spatial resolutions (Noël et al. 2018; Noël and van Kampenhout 2019; Noël et al. 2023) as well as from the Hugonnet et al. (2021) dataset of glacier integrated values. Temperature at 2-meter (t2m, hereafter) fields are taken from ERA5 and ERA5-Land (Hersbach et al., 2020; Muñoz-Sabater et al., 2021). We use Millan et al. (2022) surface ice velocity fields, except for the Antarctic (RGI 19) and Greenland (RGI 5) peripheries, where we leverage the velocity products from Mouginot et al. 2019 and Joughin et al. 2016, respectively. These datasets are the most comprehensive and up-to-date products available for glacier and ice sheet velocities. All the other features are directly imported or calculated based on datasets available from the Open Global Glacier Model (OGGM, v. 1.6.1, Maussion et al.

60

65



2023). Outside the ice sheets, we compare our model solutions with Farinotti et al. (2019)'s ensemble and Millan et al. (2022).  
70 In the Antarctic periphery (RGI 19), we compare with Farinotti et al. (2019) and BedMachine v3 (Morlighem, 2022a). In the  
Greenland periphery, we compare with Farinotti et al. (2019) and BedMachine v5 Morlighem (2022b). The latter uses Millan  
et al. (2022) for isolated glaciers and ice caps, and mass conservation or kriging interpolation elsewhere.

We employ OGGM's version (v.62) of glacier geometries, which provides a slight revision of the official Randolph Glacier  
Inventory (RGI) v. 6 version, and at the same time adds an additional 1,000 iced bodies located in the Greenland periphery  
75 with direct connection to the ice sheet, hereafter still referred to as glaciers. OGGMv62 thus provides the opportunity to also  
train and test the model ability to reproduce thickness patterns in an ice sheet flow domain, a region with an extensive amount  
of available thickness data. We point out that in this work only the thickness data contained in GlaThida has been used, rather  
than the whole set of measurements used by the two BedMachine models. OGGM glacier geometries include both the glacier  
external boundaries and the ice-free regions contained therein (hereafter referred to as nunataks). IceBoost is deployed globally  
80 on the full set of 216,502 existing glaciers as defined in OGGMv62.

A total set of 38 features are extracted from the above-mentioned datasets and used for training (Table 1). Some features  
are local, i.e., vary within the glacier, while some are per-glacier constants. The per-glacier features are: glacier area, mean  
aspect, maximum length and average slope, minimum, median, and maximum elevations, and difference between maximum  
and minimum elevation. These latter four features are directly imported from OGGM at training time, while at inference time  
85 they are calculated from Tandem-X DEMs. The 2000-2020 mean glacier mass balance values are imported from Hugonnet et al.  
(2021). We inform the model with the distance to the closest ice-free location ( $d_{noice}$ , Appendix A2) and with the distance from  
the ocean ( $d_{ocean}$ ). The model is also informed with mean annual 2-meter temperature (Appendix A7). The local elevation,  
curvature, aspect, slopes, and velocity features are described in Appendix A4.

## 2.2 Time tagging and data pre-processing

90 The datasets used in this work are tied to different time intervals. The glacier outlines refer to 2000-2010 for most glaciers  
(Pfeffer et al., 2014). The ice surface velocity outside the ice sheets is tied to 2017-2018 (Millan et al., 2022). Tandem-X  
EDEM results from acquisitions between 2011 and 2015. The GlaThiDa dataset stores ice thickness measurements from 1936  
up to 2017. The ERA5 and ERA5-Land fields are tagged to 2000-2010. To homogenize temporally as much as possible all  
datasets in the creation of the training set, while maximizing its size, all ice thickness measurements older than 2005 are  
95 discarded. In addition, we discard all measurements that lie outside glacier boundaries or inside nunataks. Overall, the model  
is conservatively estimated to be trained on data spanning from 2005 to 2017.

The resulting GlaThiDa dataset comprises 3.7 million points collected from 2300 glaciers (Fig. 1). To reduce computational  
costs, the training dataset is spatially downscaled. Each glacier is divided into a grid of 100x100 lat-lon pixels, and the per-pixel  
average is computed for all features and thickness data. The original 3.7 million point dataset is thus encoded into a 300,000  
100 point final training dataset. For comparison with existing solutions, the thickness fields of Millan et al. (2022) and Farinotti  
et al. (2019) have been similarly downscaled.





Feature	Variable name	Local	Unit	Method	Primary dataset	Note
Aspect	$a_{50}, a_{300}, a_{gfa}$	•	degrees	calculated	Tandem-X EDEM	see Appendix
Curvature	$c_{50}, c_{300}, c_{gfa}$	•	$0.01\text{m}^{-1}$	calculated	Tandem-X EDEM	see Appendix
Distance from no ice	$d_{noice}$	•	km	calculated	OGGM	see Appendix
Distance from ocean	$d_{ocean}$	•	km	calculated	GSHHG	see Appendix
Elevation	$h$	•	m	calculated	Tandem-X EDEM	see Appendix
Elevation above base	$h - H_{min}$	•	m	calculated	Tandem-X EDEM	see Appendix
Glacier area	$Area$		$\text{km}^2$	calculated	OGGM	
Glacier aspect	$Aspect$		degrees	imported	OGGM	
Glacier elevation delta	$\Delta H$		m	calculated	Tandem-X EDEM	see Appendix
Glacier length	$L_{max}$		m	imported	OGGM	
Glacier mass balance (geodetic)	$MB$		$\text{m w.e.yr}^{-1}$	imported	Hugonnet et al. (2021)	
Glacier perimeter	$Perimeter$		m	calculated	OGGM	
Glacier slope	$Slope$		-	imported	OGGM	
Glacier Type	$Form$		-	imported	OGGM	see Appendix
Glacier Terminus Type	$TermType$		-	imported	OGGM	see Appendix
Glacier min, max, median elevation	$H_{min}, H_{max}, H_{med}$		m	imported	OGGM	
Mass balance	$mb$	•	$\text{m w.e.yr}^{-1}$	calculated	RACMO2	see Appendix
Slope	$s_{50}, s_{75}, s_{100}, s_{125}, s_{150}, s_{300}, s_{450}, s_{gfa}$	•	-	calculated	Tandem-X EDEM	see Appendix
Temperature at 2 meters	$t2m$	•	K	calculated	ERA5, ERA5-Land	see Appendix
Velocity	$v_{50}, v_{100}, v_{150}, v_{300}, v_{450}, v_{gfa}$	•	$\text{m yr}^{-1}$	calculated	Millan et al. (2022) Joughin et al. (2016) Mouginot et al. (2019)	see Appendix

**Table 1.** List of features and products used by IceBoost. Local features are flagged by circles. All others are glacier mean values. The model target is the ice thickness, obtained from the GlaThiDa Consortium (GlaThiDa Consortium, 2020). See Figure 2 for an analysis of the predictive power of the features.

## 2.3 Model

We utilize two Gradient-Boosting decision Tree (GBDT) models (Friedman, 2001). A GBDT model consists of multiple additive decision trees and is trained iteratively. In each iteration, a new decision tree is added and tasked to fit the residuals of the previous tree by minimizing an objective function. Training continues until a stopping criterion is met, either reaching a maximum number of iterations or detecting overfitting through a separate validation dataset. IceBoost is an ensemble model comprising two GBDT variants: XGBoost (Chen and Guestrin, 2016) and CatBoost (Prokhorenkova et al., 2018). Both models



use a second order Taylor approximation of the objective function and employ a depth-wise tree growth scheme. However, CatBoost builds symmetric trees, which tends to act as a regularizer against overfitting, and handles categorical features natively  
110 without requiring one-hot encoding. We train both models independently using a squared loss,  $l = (y - \hat{y})^2$ , where  $y$  represents the target data from GlaThiDa and  $\hat{y}$  represent the predicted values. The IceBoost ensemble combines them by averaging their respective predictions.

Despite the different climates and glacier ice flow regimes in various regions, we decide not to specialize IceBoost regionally but rather to build one single model and optimize its hyperparameters globally. The decision is driven by the ease of deployment  
115 and the availability of certain features (particularly mass balance, temperature and distance from the ocean) that can provide some regional context to the model. It should be noted that the model optimal parameters may reflect the imbalance of the training data among different regions, potentially making it slightly more biased towards polar regions where more training data is available. Potential solutions to specializing the model regionally would include optimizing the hyperparameters separately for each region and/or applying a heavier penalty within the regions of interest.

#### 120 **2.4 Model training, hyperparameter optimization and performance**

Hyperparameter tuning is conducted independently for both XGBoost and CatBoost, both referred to as "model" for simplicity, and in an identical manner, using a Bayesian hyperparameter optimization framework (*Optuna*, Akiba et al. 2019). The best parameters are determined by training the model over  $n=200$  trials. In each trial, a different set of hyperparameters is selected, the model is trained on an 80% random split of the data, and the objective error loss is evaluated and monitored on the remaining  
125 20% split. To mitigate the risk of overfitting by tuning parameters tailored to a particular split, we randomize the 80%-20% data split in each trial. We acknowledge that typically, hyperparameter optimization is carried out by leaving out a test set for offline performance evaluation. However, given the extreme heterogeneity of the glacier regimes, thickness and feature space, we decided to find the best parameters by exposing the entirety of the data. This approach avoids the risk of overfitting by specializing the best parameters to the peculiarities of a specific part of the data considered during hyperparameter search. The trade-off of our approach is that randomizing the data splits in each trial introduces variability in the objective function. This  
130 variability can potentially make it harder to converge to the optimal hyperparameters. However, it also helps in identifying hyperparameters that generalize well across different data splits, leading to a more robust model. Additionally, variability in the loss can generally be handled in Bayesian optimization. To further prevent overfitting by reducing the model complexity, we enforce early stopping in each trial. Early stopping is a form of regularization that halts training if performance on the 20% split does not improve for  $n$  consecutive rounds, with  $n$  set to 50. The best hyperparameters are identified as those selected in  
135 the trial for which the objective loss is minimized (Appendix A8).

IceBoost performance is quantified by fixing the best set of hyperparameters, training the model and evaluating its performance regionally, using a cross-validation scheme (Table 2). Performance metrics include accuracy (median of the residual distribution  $res = GTD - IceBoost$ ) and precision (root mean squared error). Evaluation is conducted on a test set consisting  
140 of a 20% random split of the regional data. Cross-validation involves training the model  $n=100$  times, each time randomizing the regional 20% test split. Two different routines are considered to produce the 20% test split. In the first routine ('with



RGI	Region	GTD - IceBoost	rmse IceBoost w/ supervision	rmse IceBoost w/o supervision	rmse Model1 <sup>†</sup>	rmse Model2 <sup>§</sup>
1	Alaska	23 (19)	47 (2)	114 (23)	151	173
2	Western Canada and US	-	-	-	-	-
3	Arctic Canada North	-3 (4)	32 (1)	82 (6)	131	129
4	Arctic Canada South	0 (5)	18 (1)	54 (9)	103	115
5	Greenland Periphery	-5 (2)	28 (2)	80 (18)	94	95*
6	Iceland	-	-	-	-	-
7	Svalbard	0 (10)	14 (1)	52 (6)	68	59
8	Scandinavia	-1 (7)	20 (1)	42 (6)	61	54
9	Russian Arctic	-	-	-	-	-
10	North Asia	-10 (2)	4 (1)	18 (3)	19	24
11	Central Europe	-7 (4)	10 (1)	34 (5)	47	35
12	Caucasus and Middle East	16 (1)	9 (1)	54 (1)	65	56
13	Central Asia	-8 (7)	8 (1)	33 (7)	64	37
14	South Asia West	-	-	-	-	-
15	South Asia East	-	-	-	-	-
16	Low Latitudes	-	-	-	-	-
17	Southern Andes	-5 (6)	12 (1)	34 (5)	38	43
18	New Zealand	-	-	-	-	-
19	Antarctic and Subantarctic	6 (11)	47 (2)	115 (22)	119	198*

**Table 2.** IceBoost performance and comparison with existing models. All units are in meters. The numbers in parentheses refer to 1 standard deviation across n=100 cross-validation runs. GTD: GlaThiDa.

\* Glaciers from the RGI v6 repository, with no connectivity to the GrIS.

† Model 1 = Millan et al. (2022), BedMachine v5 in RGI 5 (Morlighem, 2022b), BedMachine v3 in RGI 19 (Morlighem, 2022a).

§ Model 2 = Farinotti et al. (2019).

supervision'), the 20% measurements are taken from glaciers where other data is considered for the 80% training split. This approach allows the model to be trained on one glacier data and tested on other locations within the same glacier (no data used for training is ever used for testing). In the second routine ('without supervision'), we impose a stricter constraint by creating the 20% test from completely unseen glaciers.

Due to insufficient or limited data, the evaluation of the model performance is not considered robust in regions 2, 6, 9, 14, 15, 16, and 18, hence it is not reported. Performance evaluations in regions 10, 12, 13, and 17 are considered indicative. Nevertheless, similar errors are expected for regions with comparable flow regime and mean thickness: 13-14-15, and 6-7-8-9, and 11-12-18.



150 We observe an improvement in both accuracy and precision of up to 10% across all regions when combining the predictions  
of XGBoost and CatBoost, compared to using XGBoost alone. Such an improvement supports the effectiveness of a model  
ensemble. Overall, IceBoost error is comparable to state-of-the-art global solutions outside polar regions and up to 30-40%  
lower in polar regions (Table 2). The much lower errors when training with supervision indicate that providing the model  
with glacier context proves to be beneficial. While this conclusion seems consistent on a regional scale, we find that on a  
155 glacier-by-glacier basis, the model is not always sensitive to additional tie points, regardless of where the context is provided  
(further discussion in Sect. 4). In the Greenland and Antarctic peripheries, it is noteworthy that Model 2 (Farinotti et al.,  
2019) performance is only evaluated on glaciers not connected to the ice sheet. Model 1 performance in Greenland combines  
Millan et al. 2022 shallow ice approximation for glaciers and ice caps not connected to the ice sheet, and Morlighem 2022b  
kriging/mass conservation elsewhere. In RGI 19, as ground truth data are only found in the Antarctic periphery (none in the  
160 Subantarctic islands), Model 1 is entirely BedMachine v3 (Morlighem, 2022a).

IceBoost trained modules (XGBoost and CatBoost) are deposited on Zenodo as .json and .cbm files, respectively.

### 3 Model interpretability

To understand the relative strengths of the features for the model prediction, we carry out a feature ranking analysis using  
SHapley Additive exPlanations (SHAP, Lundberg and Lee 2017). For the analysis we consider the XGBoost model. SHAP  
165 is a framework based on cooperative game theory where the goal is to equitably distribute the total gains to players (i.e.  
the model features) based on their individual contributions. A feature SHAP value reflects its marginal contribution to the  
model, specifically the change in the model's prediction when the feature is added or removed. Positive (negative) SHAP  
values indicate that the feature increases (decreases) the model prediction with respect to its average baseline (the sum of all  
SHAP values for a given instance equals the model's prediction for that instance), while SHAP absolute values represent the  
170 magnitude of the feature contribution to the model prediction, regardless of the direction.

A SHAP analysis is shown in Figure 2 for a random subset of  $n=2,000$  training data points. Each instance is represented by  
a dot. The features are ordered from top to bottom by decreasing mean absolute values, i.e. more important features are on top  
(a less informative but more compact visualization is shown in Figure A3). The feature SHAP values are the x-coordinates,  
while the feature values are represented in the color bar. As an example, points with high distance-from-ice-free regions values  
175 typically have higher SHAP values, i.e., will lead the model to higher thickness predictions. For almost all features except for  
the slope and the curvature, higher feature values will lead to higher ice thickness predictions.

Local slopes and curvature are important features, highlighting the DEM quality as a crucial input for accurate glacier thick-  
ness estimates. The elevation from the glacier minimum, rather than elevation above sea level, is found to be most informative.

The closest distance to ice-free areas is a powerful feature. Often in continental valley glaciers, the distribution of this feature  
180 mimics well the distribution of ice thickness. This feature retains its power even in large glacier systems with multiple nunataks  
(e.g., Fig. A1).

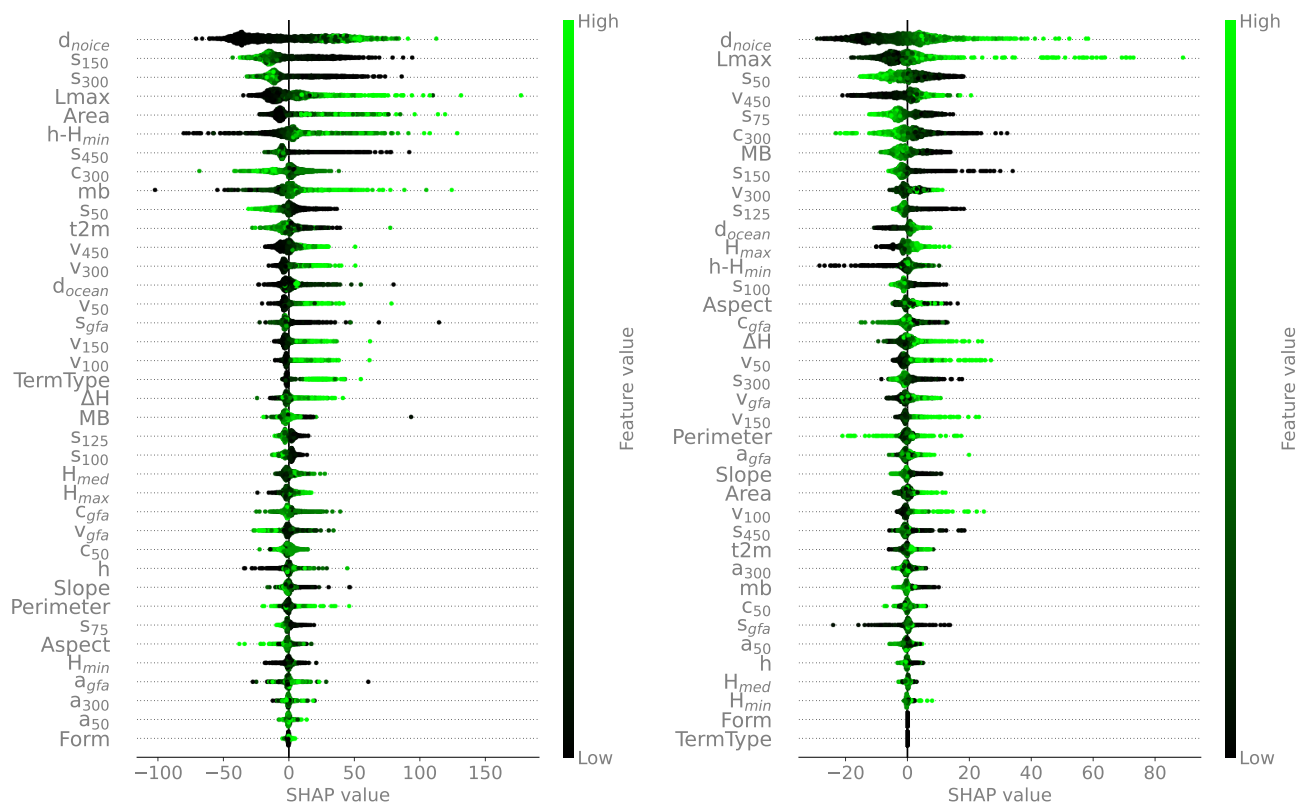


**Figure 2.** Left: SHAP analysis of  $n=2,000$  random instances (each ice measurement instance is represented by a dot on each feature row). Features are ordered from top to bottom by decreasing mean absolute SHAP values: top features are more important. The horizontal coordinate indicates how the model output changes with respect to its baseline, in a positive or negative direction, hence how predictive are the features. The color bar reflects the normalized feature variability range. See Table 1 for the variable names. Right: the same analysis is carried out on a random set of points in RGI 11 (Central Europe). See Fig. A3 for the feature rankings based solely on absolute mean SHAP values.

As known from area-volume scaling models (Bahr et al., 2015), metrics for glacier extent ( $Area$ ,  $L_{max}$ ) are found to be powerful predictors. By providing regional context for different flow regimes and glacier types, the 2-meter temperature is found to be useful. The local mass balance (Appendix A6) is also found to be relatively informative, despite our simplified approach in modeling the glacier mass balance rate of change with elevation on a regional scale. We also acknowledge that most glaciers are currently out of equilibrium, likely resulting in the accumulation and ablation zones being altered by the climate signal. Ice velocity is found to be a major predictor but, perhaps surprisingly, not as strong as those mentioned above. Possibly, the wide range of variability across over three orders of magnitude in velocity makes this information difficult to account for, in addition, possibly, to data uncertainty. The role of surface velocity is further investigated by training the model without velocity information. We find that the error increases up to 6% maximum for high-latitude regions, where most geodetic information is



relatively more constant across wider glaciers, while no substantial difference is found elsewhere. Since the largest ice volumes are stored at high latitudes, the velocity features are retained in the model.

195 Except for the metrics related to glacier size, all other glacier-integrated features (see Table 1) are found to be relatively unimportant, including glacier geodetic mass balance values. Regional context related to glacier locations and metrics of continentality, derived from temperature and distance to the ocean, are found to be moderately informative, but significantly less so than local geodetic information. Overall, the analysis highlights the crucial importance of high-quality DEMs.

200 The analysis provides a general overview of the predicting power of the feature set by accounting for a random set of training points. A slight reshuffling of the feature ranking is expected if evaluating glaciers individually or regionally (e.g., RGI 11 in Fig. 2). Some features are consistently found to be relatively uninformative and can be dropped without loss of predicting power. The local aspect features ( $a_{50}$ ,  $a_{300}$ ,  $a_{gfa}$ ) as well as the glacier type feature *Form* are dropped hereafter. The total number of features retained by IceBoost is therefore 34.

#### 4 Model deploy

At deploy time, the model ensemble is tasked to produce a continuous glacier ice thickness solution. The pipeline consists in generating  $n$  discrete points randomly inside the glacier boundary and outside nunataks, calculating the feature vector  $\mathbf{x}_n$  and querying the model locally  $h_n = \text{IceBoost}(\mathbf{x}_n)$ . The feature vector  $\mathbf{x}_n$  is calculated on-the-fly (Appendix, B1). The glacier volume is calculated by Monte Carlo approximation (Appendix, B3). An approximately continuous solution can be obtained in the limit  $\lim_{n \rightarrow \infty} h_n(\mathbf{x}_n)$ . Typically  $n = 10,000$  provides a good representation even for relatively big glaciers.

210 To investigate the effect of added supervision, we consider the Malaspina glacier (RGI60-01.13696). The glacier, located in coastal southern Alaska, is the world's largest piedmont glacier with an area of 3900 km<sup>2</sup>. The terminus is largely grounded below sea level. Measurements on this glacier are found in our training dataset. A recent campaign has vastly increased the amount of measurements on the glacier and provided a detailed overview of the terminus thickness distribution and bedrock topography (see Fig. 5 in Tober et al. 2023).

215 We train the model with and without the available measurements included in the training dataset (hereafter referred to as "with and without supervision", respectively). We point out that, contrary to a kriging technique, IceBoost does not use the data explicitly, but rather adjusts its parameters at training time. The model trained without supervision predicts an ice thickness of up to 700-800 m at the terminus and in other deepest parts of the glacier. Next, we include the measurements in the training set and train the model with supervision. The model output changes drastically at the terminus, with the solution values closer to the ground truth, although the model still struggles to fully capture the high thickness values that correspond to localized deep subglacial channels found by radar surveys (Tober et al., 2023). Note that the solution changes in other parts of the terminus as well and also relatively far from the data. Training IceBoost with supervision greatly improves the model skill, suggesting that a significant advantage compared to existing approaches is achieved when data is available by: i) improving the general model performance by increasing the training data; and ii) improving the prediction on individual glaciers. While it is not trivial to understand why IceBoost prediction without supervision deviates from the ground truth for the Malaspina Glacier, the model



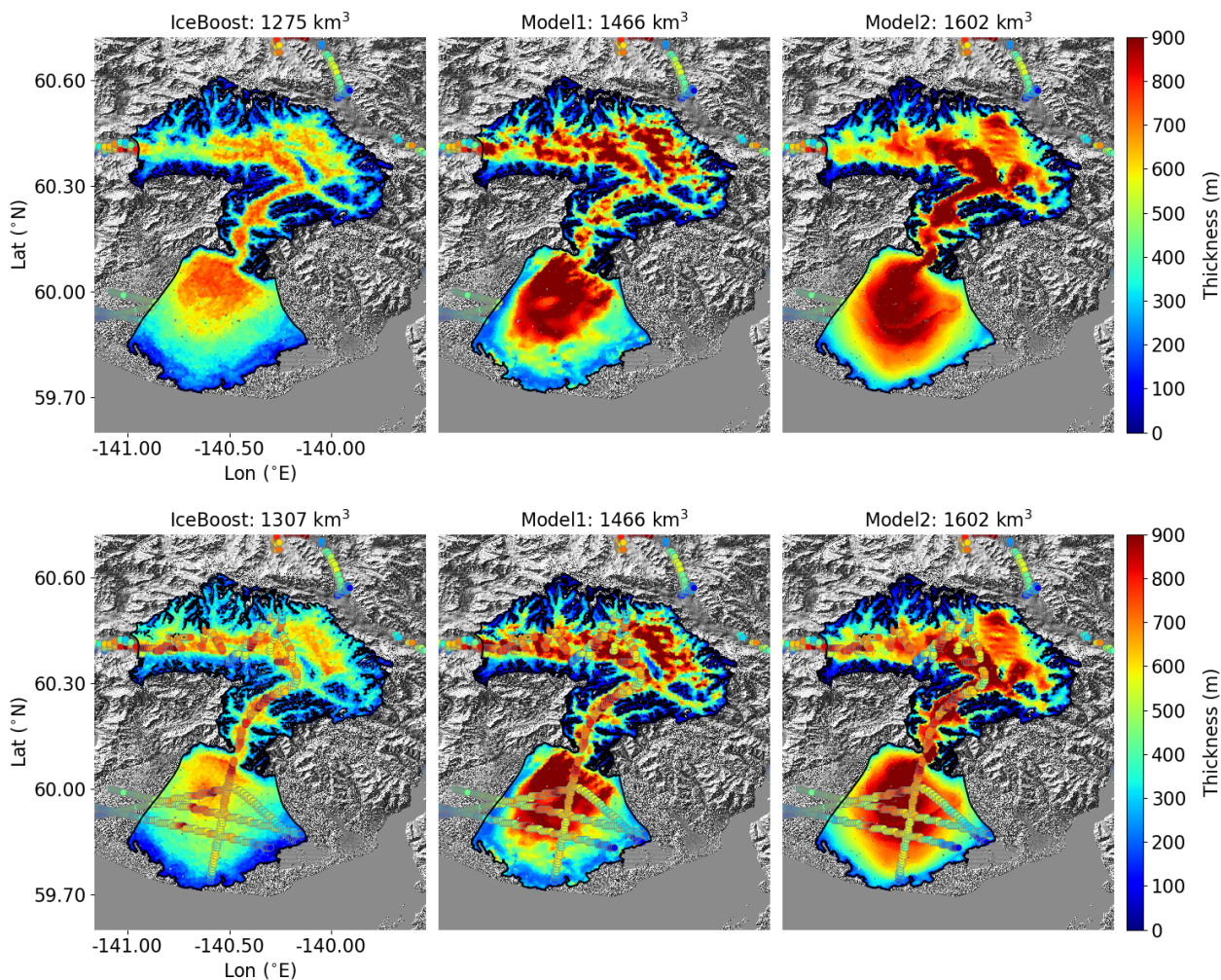


**Figure 3.** Modeling of the Malaspina glacier (RGI60-01.13696) by IceBoost (this work), Millan et al. 2022 (Model1) and Farinotti et al. 2019 (Model2). IceBoost is trained without supervision (top) and with supervision (bottom). The difference in predicted volumes is 3.9%. The circles reflect the measurements.

error is consistent with what has been found in this region at cross-validation (RGI 1, Table 2). This experiment also shows that, although the model does not account for an explicit dependence between points (opposite to a neural network structure), the model produces a meaningful covariant pattern.

Although adding supervision has shown to increase solution accuracy for the Malaspina Glacier, we conclude that in general, adding supervision does not change the solution substantially, and the model is able to generalize well. Thus, the error reduction shown in Table 2 likely reflects an improvement in performance of modeling deep glaciers with a rather complicated feature





230 space. As an example, the same analysis carried out for Mittie Glacier, a large and surge-type glacier in Arctic Canada N. (Fig. 4) shows that training with or without supervision does not change the model prediction substantially.

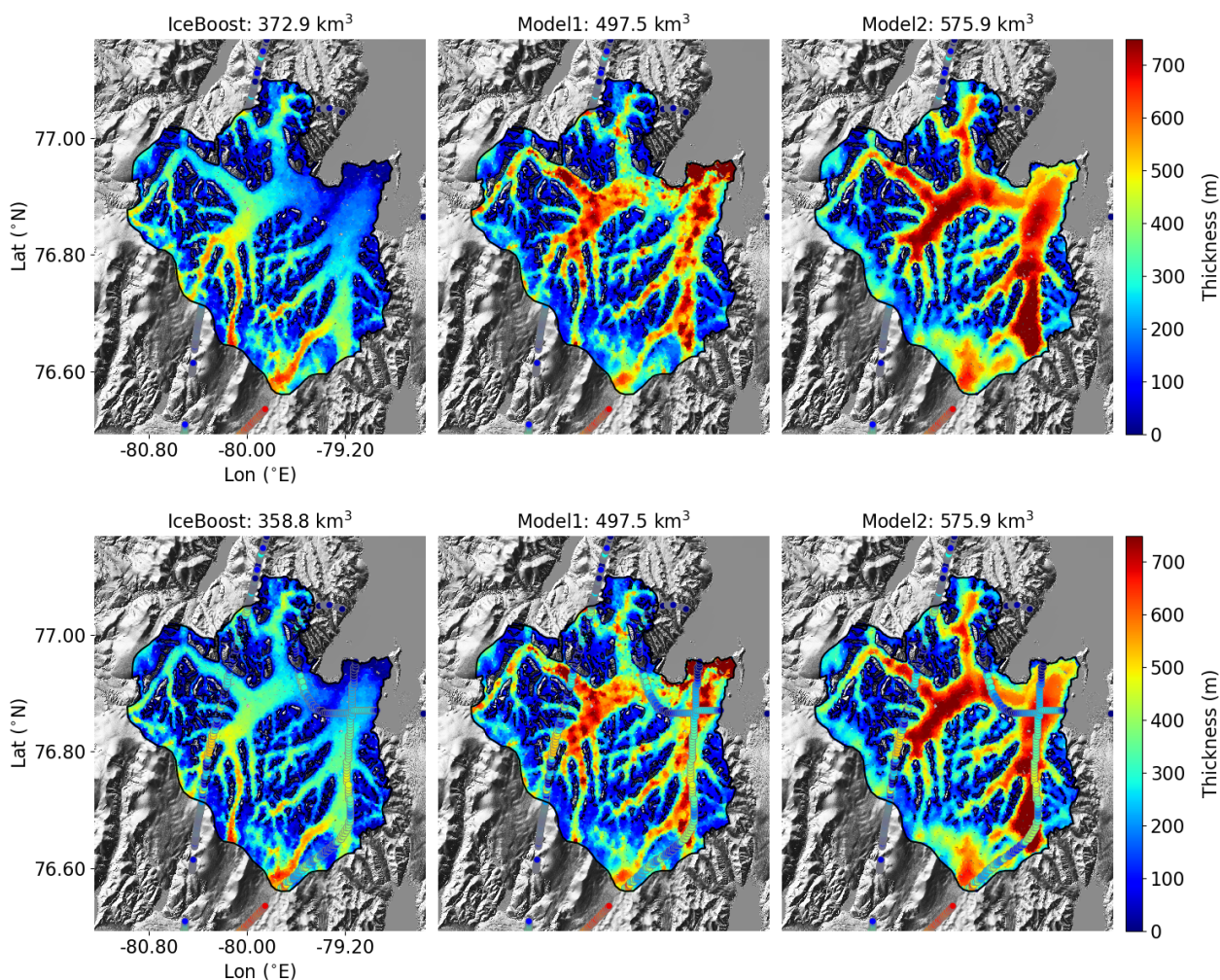


**Figure 4.** Modeling of Mittie Glacier (RGI60-03.01517, Arctic Canada N.) by IceBoost, Millan et al. 2022 (Model1) and Farinotti et al. 2019 (Model2). IceBoost is trained without (top) and with supervision (bottom). The difference in predicted volumes is 3.8%. The circles reflect the measurements.

The satellite products used by IceBoost have different spatial resolution, ranging from 30 m (DEM) up to 250 m for surface velocity fields over the ice sheets. Convolution with various kernels of different size are also implemented when generating the features, enlarging the receptive field. Conversely, the features not based on satellite products are not discrete. The minimal spatial variation of the thickness distributions generated by IceBoost, loosely referred to as the model resolution, is evaluated by visually assessing the predictions (examples in Figures 5), and is estimated to be  $\simeq 100$  m. The model has neither the



capabilities (it is not trained to) nor the resolution to predict smaller-scale basal features, unless their fingerprints are captured on the surface.

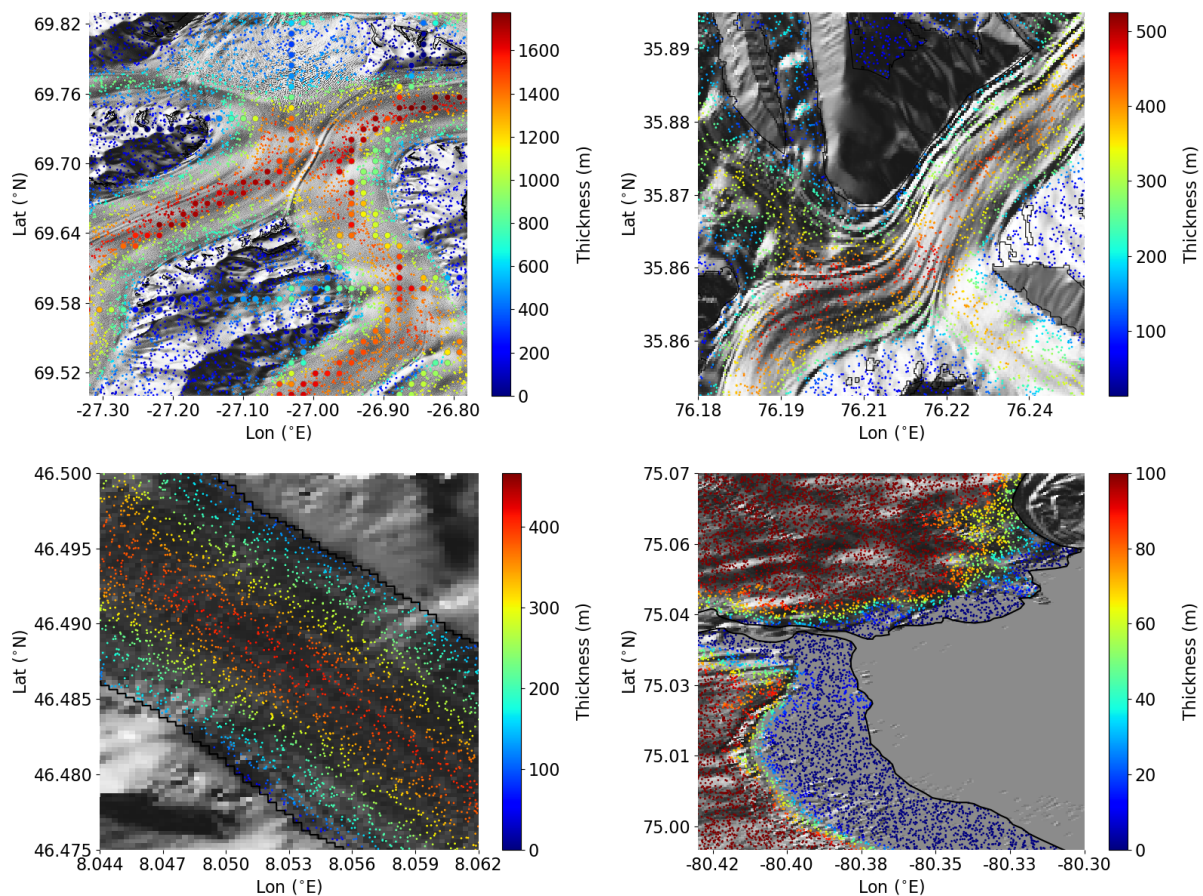


**Figure 5.** IceBoost solutions across different spatial scales. From top left in clockwise order: RGI60-05.13501 (Greenland, big circles are thickness measurements), RGI60-14.06580 (Yanatsugat glacier, Karakoram range), RGI60-03.02467 (Devon Ice Cap, Arctic Canada), RGI60-11.01450 (Aletsch glacier, Swiss Alps, Central Europe). Zoom in for best view.

The model is able to predict rather fine-grained details, such as glacier front transitions to ice shelves across marine terminating glaciers (e.g. Devon Ice cap, Fig. 5), likely informed by the following features:  $d_{ocean}$ ,  $h - H_{min}$ ,  $TermType$ , curvature, and slope.

#### 4.1 Comparison with existing global models

A more extensive comparison between IceBoost and other models is found in the Supplementary Information, released on Zenodo at <https://doi.org/10.5281/zenodo.13145836>. We produce the ice distribution for 10 glaciers in each one of the 19 RGI



245 regions. In every plot, Model1 refers to Millan et al. 2022 or BedMachine (RGI 5: Morlighem 2022b, RGI 19: Morlighem 2022a); Model2 refers to Farinotti et al. 2019.

## 5 Computational cost

The memory load for creating the training dataset is 80 Gbytes, primarily due to memory necessary to import, merge and operate on the DEM tiles. Downgrading to Tandem-X 90m would certainly reduce the computational cost, at the expense of accuracy. Model training and deploy is done on GPU; however, it can be easily run on CPU. Model training requires a few minutes. The inference time, ca. 0.06 s for XGBoost and 0.03 s for CatBoost, is almost completely driven by the generation of features arrays, which is carried out on 20 CPUs with parallelization wherever applicable: for  $n = 10^4$  query points, the time required varies between 1 second to 1 minute for the most complex glaciers. If higher spatial details is needed, the point density can be selectively increased locally up to  $O(10^5)$ . We recommend not increasing  $n$  above a million points as the information gain is limited by the model resolution ( $\simeq 100$  m). Hard disk memory recommendations are 10-500 Gbytes. All of Earth's glaciers can be conservatively run on 1 Tbytes hard disk, 128 Gbytes RAM and 1-20 CPUs. A graphics card is not necessary.

## 6 Conclusions

IceBoost is to the best of our knowledge the first machine-learning based approach able to estimate the ice thickness distribution of all Earth's glaciers. The model operates using a set of 34 numerical features; its parameters are optimized globally. As typical of machine learning methods, the model performance will improve by increasing the dataset size. Future measurement campaigns will be beneficial for the training dataset. The large amount of training data available at high latitudes and the model errors in these regions suggest that, for our modeling approach, providing more data is more beneficial than providing more accurate data. In the ice sheet peripheries, IceBoost is only trained with those measurements included in the GlaThiDa dataset, and does not leverage the whole set of existing measurements. Extending the training with all available measurements is expected to further improve IceBoost. However limited, the comparison with BedMachine demonstrates the skills of the machine-learned approach also in this region. We summarize the following conclusions:

- The model error is similar to state-of-the-art models in mid-to-low latitude glaciers, and up to 30-40% lower at high latitudes.
- Providing supervision (i.e. measurements) further reduces the model error by roughly a factor  $\simeq 2$  to 3. Measurement campaigns targeting deep ice zones would prove extremely beneficial for improving IceBoost estimates of ice volumes. However, we find that not all glaciers benefit equally from added supervision.
- With the exception of DEMs which are available at high resolution and increasing accuracy, our modeling approach is not hard-constrained by the availability of specific input feature, notably ice velocity. The imputation policies enable the production of skillful thickness distributions even when some input features are completely unavailable. Ice velocity





275 improves the model by up to 6% at high latitudes, though no improvement is found elsewhere. Despite its marginal impact, this area holds the majority of the Earth ice volume.

- The most informative features are the distance to ice-free regions, surface slopes, surface curvature, and metrics of glacier size. An improved mass balance feature will likely improve the model performance. We consider that our current local mass balance feature is only a simplified estimate.

280 *Code and data availability.* IceBoost v1 source code and trained model is released on GitHub: <https://github.com/nmaffe/iceboost>, and on Zenodo at <https://doi.org/10.5281/zenodo.13145836>. On Zenodo we also archive the Supplementary material: the training data, the final trained model (.json and .cbm), the model outputs on selected glaciers, alongside the comparisons with other models discussed in the text.

*Author contributions.* N.M. conceived and designed the research. N.M., E.R., S.V., T.P contributed to the development of the input feature set. N.M. wrote the model pipeline, performed the experiments and analyzed the results, with inputs from all authors. N.M. drafted the  
285 manuscript, to which all the authors contributed.

*Competing interests.* The authors declare that they have no conflict of interest.

*Acknowledgements.* We would like to thank Gianluca Lagnese for valuable and constructive discussions. We thank the following students from the Niels Bohr Institute - Applied Machine Learning 2024 class for their valuable ideas, analyses and parameter optimization: Emma Hvid Møller, Marcus Benjamin Newmann, Cerina von Bruhn, Jonas Richard Damsgaard, Josephine Gondán Kande, Luisa Elisabeth Hirche  
290 and Simon Wentzel Lind. This work has received funding from the European Union’s Horizon 2020 research and innovation programme, under the Marie Skłodowska-Curie grant agreement No 101066651. This work was also funded by the Climate Change AI Innovation Grants program, hosted by Climate Change AI with the additional support of Canada Hub of Future Earth, under the project name ICENET.



## Appendix A: Training features

### A1 Glaciery Type (*Form*) and and Terminus Type (*TermType*)

295 Both features are extracted from OGGM. The values are discrete:

- **Form** = { '0': 'Glacier', '1': 'Ice cap', '2': 'Perennial snowfield', '3': 'Seasonal snowfield', '9': 'Not assigned' }.
- **TermType** = { '0': 'Land-terminating', '1': 'Marine-terminating', '2': 'Lake-terminating', '3': 'Dry calving', '4': 'Re-generated', '5': 'Shelf-terminating', '9': 'Not assigned', }.

### A2 Distance from ice free regions ( $d_{noice}$ )

300 Given a point  $x$  inside a glacier  $g$ , we calculate the distance to the closest free pixel. Such a target point may lie within or outside the glacier.

We define a glacier cluster as the collection of all neighboring glaciers. For example, three glaciers  $\{g_1, g_2, g_3\}$  form a cluster if  $g_1$  shares a pixel with  $g_2$  and  $g_2$  shares a pixel with  $g_3$ , despite  $g_1$  and  $g_3$  not being adjacent glaciers.

The glacier cluster is calculated by detecting, starting from the glacier that contains the point  $x_0$ , all its proximal neighbors.  
305 The procedure is repeated iteratively for every neighboring glacier until no further neighbors are found. Once the cluster is computed, all internal shared borders (the ice divides) of the cluster are removed, while internal ice-free nunataks are kept. This procedure potentially results in collections of up to thousands of geometries per cluster (Fig. A1).

The minimum distance from the point  $x_0$  to an ice-free region ( $d_{noice}$ ) is the minimum of distance between  $x_0$  and all points  $x$  lying on the cluster's valid geometries.

$$310 \quad d_{noince}(x_0) = \operatorname{argmin}_x d(x_0, x), x \in cluster \quad (A1)$$

The valid geometries can either be the cluster's external boundaries or all the cluster's nunataks. The distances are computed by querying K-dimensional trees, an approximate nearest neighbor lookup method, on the geometries defined in the Universal Transverse Mercator (UTM) projection. We compare the proximal points obtained from this method with those from a brute-force calculation and find indiscernible results. The pipeline is computed both as a feature for the creation of the training dataset  
315 and at inference time for every generated point. For computational speedup, at inference time, the number of geometries K used by the KD-tree can be capped to 10,000.

### A3 Distance from the ocean ( $d_{ocean}$ )

Similar to the distance to ice-free regions, we calculate the closest distance to the ocean. We use the Global Self-consistent, Hierarchical, High-resolution Geography Database (GSHHG), containing all the world's shoreline geometries, in resolution  
320 "f" (full). Like  $d_{noice}$ ,  $d_{ocean}$  is calculated by querying a KD-tree on the geometries, in UTM projection. We find this feature to be relatively unimportant on continental glaciers far from the coasts, but increasingly informative at high latitudes.

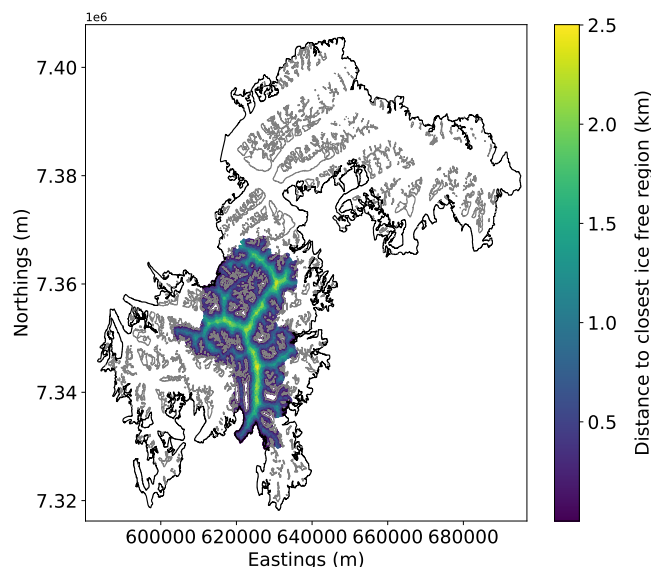


**Figure A1.** The feature  $d_{noice}$  is shown for glacier 'RGI60-05.13995', South East Greenland. The cluster external geometry with ice divides removed is shown in black. All cluster nunatak geometries are shown in grey.

#### A4 Geodetic features: elevation, aspect, curvature and slope

We use Tandem-X EDEM to calculate the following features: local elevation  $h(x, y)$ , elevation above the glacier lowest elevation  $h_{gl,min}$ , aspect, curvature and slope. The elevation above the glacier lowest elevation is simply obtained by subtracting the elevation to the glacier lowest elevation:  $h(x, y) - h_{gl,min}$ . The elevation delta  $\Delta H$  is the glacier elevation difference between minimum and maximum.

To calculate the slopes, the elevation tiles are first projected in UTM, differentiated and the resulting vector magnitude is convoluted using Gaussian filters of different kernel widths to capture the variability across different spatial scales: 50m, 75m, 100m, 125m, 150m, 300m, 450m and an adaptive filter  $af$ , Eq. A2:

$$330 \quad af = \frac{A}{\pi 0.5 L_{max}} \quad (A2)$$

where  $A$  and  $L_{max}$  are the area and glacier maximum length features. This kernel aims at estimating the glacier spatial size. For values lower than 100 or above 2000 meters,  $af$  is constrained to these values. Each training point entry results in eight slope features. The purpose of using an array of kernels is to allow the model the freedom to account for different glacier spatial scales. For small glaciers the small kernels are found to be more important than the bigger kernels, and vice versa.

335 To limit the computational cost, for the calculation of the aspect and the curvature, the elevation field is smoothed using only the 50m and 300m kernels, thus resulting in 2 + 2 features per point. All geodetic features are obtained from linear interpolation.



## A5 Velocity

The velocity magnitude field is smoothed with the six kernels: 50m, 100m, 150m, 300m, 450m and *a.f* and linearly interpolated.  
340 The velocity products used have different resolution: Millan et al. (2022) (all regions except for Greenland and Antarctica),  
Joughin et al. (2016) (Greenland) and Mouginot et al. (2019) have resolutions of 50m, 250 and 450 meters, respectively. If  
the product resolution is higher than any kernel size, the kernels are set to match the product resolution. For every training  
point a total of six velocity features are obtained. At inference time, the missing velocity features are treated according to the  
imputation policy described in Appendix B2.

## 345 A6 Mass balance

### A6.1 Polar ice sheet peripheries

In addition to glacier-averaged mass balance data from Hugonnet et al. (2021), we inform the model with local mass balances  
values. For the Greenland and Antarctic peripheries, we leverage the RACMO2 (Noël et al., 2018) product versions, down-  
scaled, respectively, to 1 km (Noël and van Kampenhout, 2019) and 2 km (Noël et al., 2023). Before linearly interpolating the  
350 mass balance fields, we i) compute the time average over the 1961-1990 and 1979-2021 time periods respectively, and ii) fill  
some gaps in the dataset by convolving with Gaussian kernels of 1 km and 2 km respectively. Few gaps still remain in the mass  
balance fields, along some areas and glaciers (sub Antarctic islands and a few glaciers off the coasts of the Antarctic peninsula)  
not covered by these datasets. For these areas, as well as for all other glaciers, we use the approach described below.

### A6.2 Glaciers outside polar ice sheets

355 For all glaciers outside the Greenland and Antarctic peripheries, we use the 2000-2020 mean glacier-integrated mass balance  
values from Hugonnet et al. (2021) and estimate the local variability by downscaling using approximate elevation-mass balance  
rates. In particular, for all glaciers within the same region, we assume a linear variation of mass balance with elevation:

$$y = s \cdot h + q \tag{A3}$$

where  $y$  is the mass balance and  $h$  is the elevation.  $s$  expresses the rate of change of mass balance with elevation, while  $q$   
360 reflects the mass balance at zero elevation. For any pairs of glaciers:

$$y_1 = s_1 \cdot h_1 + q_1 \tag{A4}$$

$$y_2 = s_2 \cdot h_2 + q_2 \tag{A5}$$





By using the glacier mean values  $mb = \bar{y}$  from (Hugonnet et al., 2021) and further assuming that for close glaciers  $s_1 = s_2 = m$  and  $q_1 = q_2 = q$ , we obtain:

$$365 \quad s = \frac{mb_1 - mb_2}{\bar{h}_1 - \bar{h}_2} \quad (\text{A6})$$

$$q = mb_1 - s\bar{h}_1 = mb_2 - s\bar{h}_2 \quad (\text{A7})$$

For a given a glacier  $i$ , compute its mean rate  $s_i$  by extending the calculation in Eq. A6 to all the other glaciers in the region  $j \neq i$ , weighting the mean by the inverse of the glacier distances:

$$s_i = \frac{\sum_{i \neq j} \frac{\Delta mb_{ij}}{\Delta h_{ij}} \cdot \frac{1}{d_{ij}^2}}{\sum_{i \neq j} \frac{1}{d_{ij}^2}} \quad (\text{A8})$$

$$370 \quad q_i = mb_i - s_i \bar{h}_i \quad (\text{A9})$$

where  $\Delta mb_{ij} = mb_i - mb_j$  and  $\Delta h_{ij} = \bar{h}_1 - \bar{h}_2$  are the differences in glacier mass balance and average elevation between glacier  $i$  and some glacier  $j$ , while  $d_{ij}$  is the distance between the two glacier center values.

As an example, the distribution of  $(s_i, q_i)$  calculated for all glaciers in RGI 11 (Central Europe, 3927 glaciers) is shown:

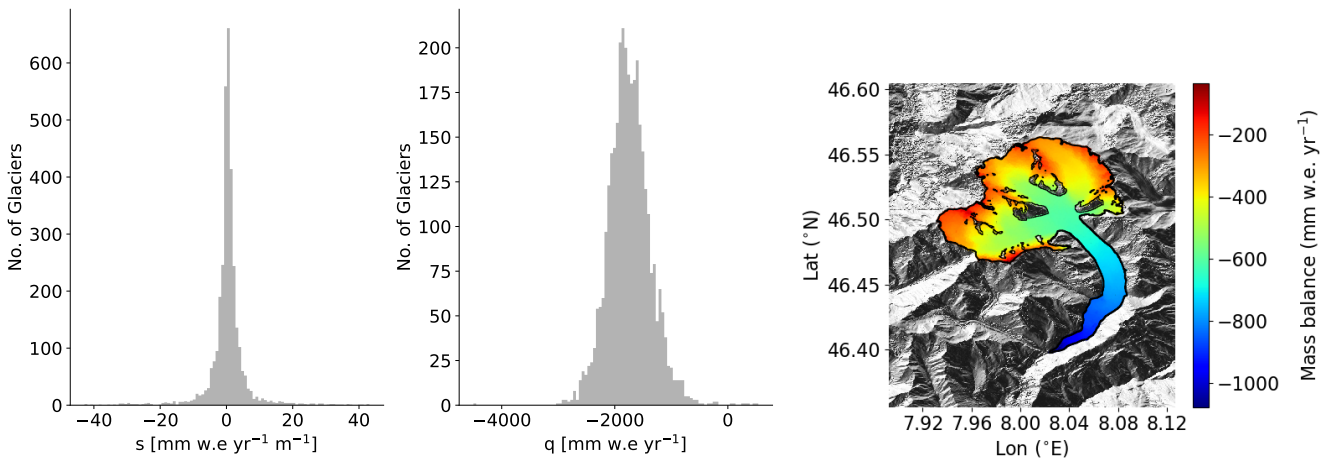


**Figure A2.** Distribution of  $(s_i, q_i)$  for RGI 11 along with the mass balance distribution for the Aletsch glacier.

To compute mass balance maps for each glacier in each region, we use the regional mean values  $\bar{s}$  and  $\bar{q}$ , listed in Table A1.  
 375 Using this method we can replicate the glacier-integrated mass balance values (Hugonnet et al., 2021) within a factor  $\approx 2$ -3.  
 Given all the hypotheses made, we consider our downscaling approach as an attempt to provide the model with crude, yet local, mass balance approximations.



RGI	1	2	3	4	5	6	7	8	9	10
$\bar{s}$ (mm w.e. yr <sup>-1</sup> m <sup>-1</sup> )	0.46	0.34	0.22	0.65	0.55	0.84	0.86	0.56	0.64	0.30
$\bar{q}$ (mm w.e. yr <sup>-1</sup> )	-1038	-1019	-485	-879	-703	-1082	-524	-1088	-405	-1034
RGI	11	12	13	14	15	16	17	18	19	
$\bar{s}$ (mm w.e. yr <sup>-1</sup> m <sup>-1</sup> )	0.41	0.14	0.46	0.16	0.32	0.52	0.45	0.14	0.41	
$\bar{q}$ (mm w.e. yr <sup>-1</sup> )	-1739	-919	-1956	-919	-2054	-2889	-1051	-440	-191	

**Table A1.** Regional values of  $\bar{s}$  and  $\bar{q}$ .

## A7 Temperature

Local 2m temperature (t2m) is added as feature to the training data. We use ERA-5 Land (0.1 degree grid spacing, Muñoz-Sabater et al. 2021) and, for the missing pixels caused by imperfect fractional land masks along the coastlines and islands, we incorporate the ERA5 t2m field (0.25 degree resolution, Hersbach et al. 2020), bilinearly interpolated to 0.1 degree resolution. We consider monthly maps averaged over the 2000-2010 time period to generate one single global temperature field, which is linearly interpolated the at the measurement points (training) or at the generated points (inference time).

## A8 IceBoost hyperparameters

The best XGBoost hyperparameters found during the Bayesian optimization pipeline are: tree\_method=hist, lambda=76.814, alpha=76.374, colsample\_bytree=0.9388, subsample=0.741501, learning\_rate=0.079244, max\_depth=20, min\_child\_weight=19, gamma=0.18611. We use 1000 trees (num\_boost\_round) with early\_stopping\_rounds=50. For CatBoost: iterations=10,000, early\_stopping\_rounds=50, depth=6, learning\_rate=0.1. For the parameter description, we refer to the XGBoost documentation at <https://xgboost.readthedocs.io/en/stable/parameter.html> and CatBoost at <https://catboost.ai/en/docs/concepts/parameter-tuning>.



390 **A9 Mean absolute SHAP values**

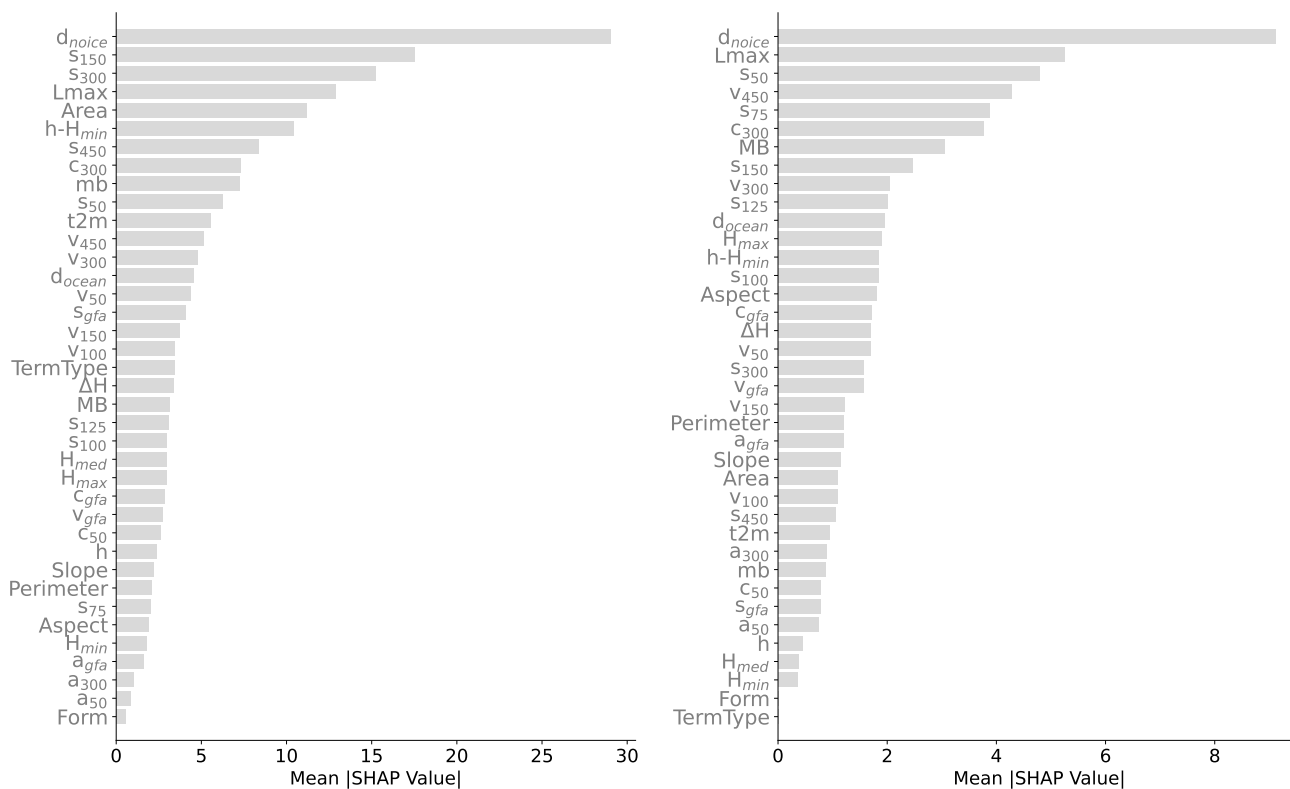


**Figure A3.** Global feature importance plot: the importance of each feature is taken to be the mean absolute shape value for that feature over  $n=2,000$  random samples (left) and over  $n=2,000$  samples from Central Europe (RGI 11, right).



## Appendix B: Model inference

### B1 Fetching features on-the-fly

At inference time, the features are generated on-the-fly following the same pipeline described for the creation of the training set. As an example, Figure B1 shows the extraction of the  $v_{50}$  feature for  $n=1500$  random points.

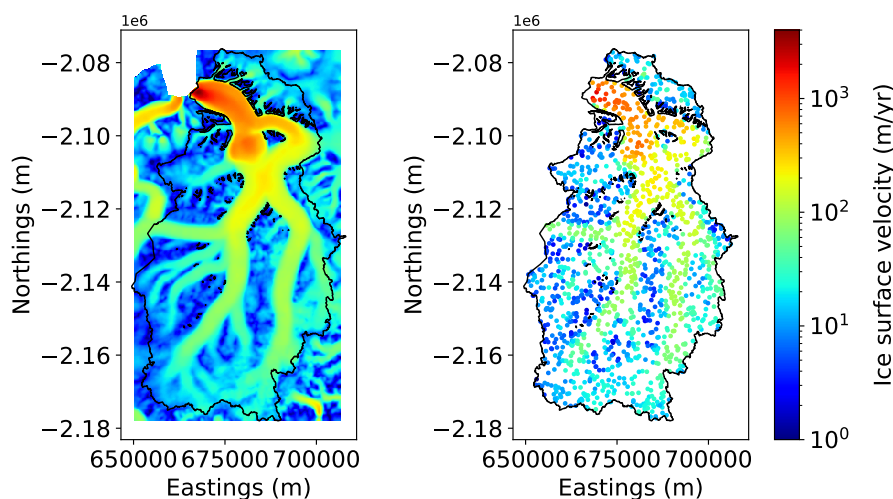


**Figure B1.** Pipeline for feature generation at inference time. Left: ice velocity ( $v_{50}$ , from Joughin et al. (2016) over glacier RGI60-05.13501 in East Greenland. Right: feature calculated for  $n=1500$  random points.

### 395 B2 Feature imputation policies

Feature imputation is need whenever any feature is not available either for the creation of the training dataset or at inference time. Unless specified, we adopt the same policy in both cases. Hereafter is a list of the features that may require imputation and their imputation policies.

#### Glacier aspect

400 The glacier aspect is set to zero.

#### Glacier length

If no glacier length is available from OGGM, it is calculated by first reprojecting the glacier external geometry in UTM coordinates, then by calculating the the matrix of pairwise distances and extracting the maximum using a KD-tree.

#### Glacier mass balance (geodetic)

405 The Hugonnet et al. (2021) mass balance dataset is tied to the RGI v.6 glacier dataset, while we use OGGM's v. 62 extension. We impute the missing glaciers with a regional median value.

#### Glacier median elevation



$H_{med}$  values are extracted from OGGM, and quite a few data is missing. At training time the glacier median elevation is imputed as the average between the glacier minimum and maximum elevations. At inference time no imputation is needed since  
410 this feature is calculated directly from Tandem-X EDEM.

#### Ice velocity

No imputation is implemented at training time: if any velocity feature is missing at any point, the point is not included in the training dataset. This condition occurs if the training point falls outside the velocity field (old measurement or measurement inside a nunatak or incomplete velocity coverage) or if it is too close to the geometry such that the interpolation fails. At infer-  
415 ence time, a complete velocity feature coverage is required as input for the model. A 3-layer progressive policy is implemented to fill any missing data and ensure complete coverage of all velocity features: i) kernel-based interpolation using a Fast Fourier Transform convolution and Gaussian kernels, ii) glacier-median imputation and iii) regional-median imputation.

#### Mass balance

The RACMO products used for Greenland and Antarctica do not cover some glaciers located on islands far from the ice sheets.  
420 These include almost all glaciers from the sub-Antarctic islands. For these, we use the downscaling approach described in Appendix A6.2.

### **B3 Glacier volume calculation**

The glacier volume is approximated by Monte Carlo as  $V_{gl} = A_{gl} N^{-1} \cdot \sum_{x,y} h(x,y)$ , where  $A_{gl}$  is the glacier area,  $h(x,y)$  is the modelled thickness at point  $(x,y)$  inside the glacier,  $N$  is the total number of generated points. This method, tested by  
425 comparing Farinotti's interpolated thickness values against their true values allows to estimate the Monte Carlo error to less than 1%, even for the biggest glaciers. While  $N = 10^4$  allows for a precise volume estimate, to better evaluate the spatial variability of the solution over scales of tens of meters,  $N$  can be increased to  $O(10^5)$ , depending on glacier size, or increased locally to target specific regions.



#### B4 Comparison with BedMachine Greenland

430 Figure B2 shows a comparison between IceBoost and BedMachine (Morlighem, 2022b) for a glacier with direct connection to the ice sheet. Note the additional complexity of the fjord system predicted by IceBoost, compared to BedMachine. While an extensive comparison with BedMachine is beyond the scope of this work, we highlight the potential of IceBoost in the ice sheet peripheries as well.

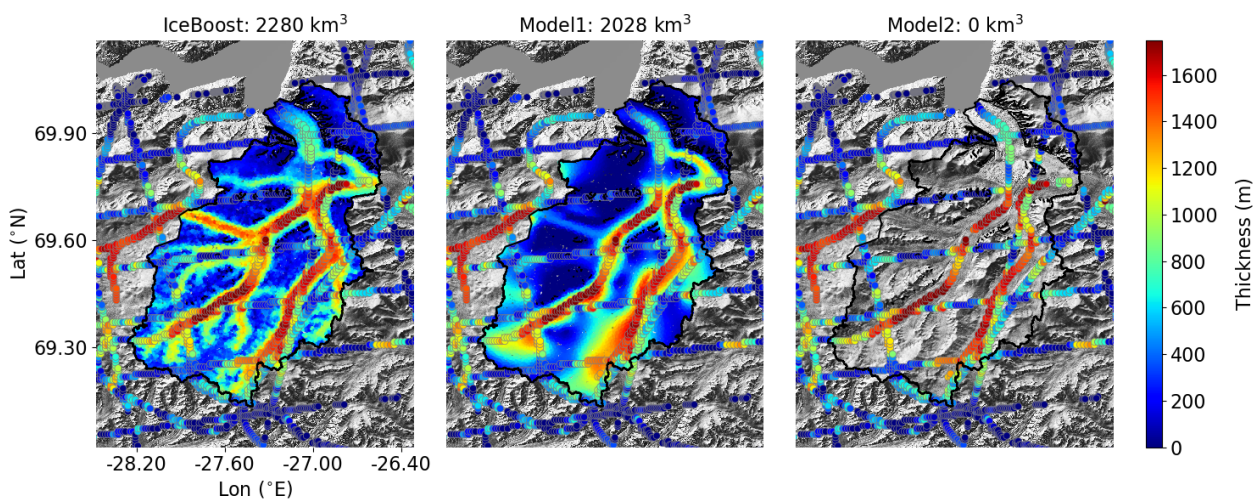


**Figure B2.** Glacier RGI60-05.13501 modeled by IceBoost, and BedMachine v5 (Model1, Morlighem 2022b). Model2 (Farinotti et al., 2019) is not available.



## References

- 435 Akiba, T., Sano, S., Yanase, T., Ohta, T., and Koyama, M.: Optuna: A Next-generation Hyperparameter Optimization Framework, in: Proceedings of the 25th ACM SIGKDD International Conference on Knowledge Discovery and Data Mining, 2019.
- Bahr, D. B., Pfeffer, W. T., and Kaser, G.: A review of volume-area scaling of glaciers, *Reviews of Geophysics*, 53, 95–140, 2015.
- Bueso-Bello, J.-L., Martone, M., González, C., Sica, F., Valdo, P., Posovszky, P., Pulella, A., and Rizzoli, P.: The global water body layer from TanDEM-X interferometric SAR data, *Remote Sensing*, 13, 5069, 2021.
- 440 Chen, T. and Guestrin, C.: Xgboost: A scalable tree boosting system, in: Proceedings of the 22nd acm sigkdd international conference on knowledge discovery and data mining, pp. 785–794, 2016.
- Clarke, G. K., Berthier, E., Schoof, C. G., and Jarosch, A. H.: Neural networks applied to estimating subglacial topography and glacier volume, *Journal of Climate*, 22, 2146–2160, 2009.
- Cuffey, K. M. and Paterson, W. S. B.: *The physics of glaciers*, Academic Press, 2010.
- 445 Farinotti, D., Brinkerhoff, D. J., Clarke, G. K., Fürst, J. J., Frey, H., Gantayat, P., Gillet-Chaulet, F., Girard, C., Huss, M., Leclercq, P. W., et al.: How accurate are estimates of glacier ice thickness? Results from ITMIX, the Ice Thickness Models Intercomparison eXperiment, *The Cryosphere*, 11, 949–970, 2017.
- Farinotti, D., Huss, M., Fürst, J. J., Landmann, J., Machguth, H., Maussion, F., and Pandit, A.: A consensus estimate for the ice thickness distribution of all glaciers on Earth, *Nature Geoscience*, 12, 168–173, 2019.
- 450 Friedman, J. H.: Greedy function approximation: a gradient boosting machine, *Annals of statistics*, pp. 1189–1232, 2001.
- GlaThiDa Consortium, Zurich, S.: Glacier Thickness Database 3.1.0. World Glacier Monitoring Service, <https://doi.org/10.5904/wgms-glathida-2020-10>, 2020.
- González, C., Bachmann, M., Bueso-Bello, J.-L., Rizzoli, P., and Zink, M.: A fully automatic algorithm for editing the tandem-x global dem, *Remote Sensing*, 12, 3961, 2020.
- 455 Grinsztajn, L., Oyallon, E., and Varoquaux, G.: Why do tree-based models still outperform deep learning on typical tabular data?, *Advances in neural information processing systems*, 35, 507–520, 2022.
- Hersbach, H., Bell, B., Berrisford, P., Hirahara, S., Horányi, A., Muñoz-Sabater, J., Nicolas, J., Peubey, C., Radu, R., Schepers, D., Simmons, A., Soci, C., Abdalla, S., Abellan, X., Balsamo, G., Bechtold, P., Biavati, G., Bidlot, J., Bonavita, M., De Chiara, G., Dahlgren, P., Dee, D., Diamantakis, M., Dragani, R., Flemming, J., Forbes, R., Fuentes, M., Geer, A., Haimberger, L., Healy, S., Hogan, R. J.,
- 460 Hólm, E., Janisková, M., Keeley, S., Laloyaux, P., Lopez, P., Lupu, C., Radnoti, G., de Rosnay, P., Rozum, I., Vamborg, F., Villaume, S., and Thépaut, J.-N.: The ERA5 global reanalysis, *Quarterly Journal of the Royal Meteorological Society*, 146, 1999–2049, <https://doi.org/https://doi.org/10.1002/qj.3803>, 2020.
- Hugonnet, R., McNabb, R., Berthier, E., Menounos, B., Nuth, C., Girod, L., Farinotti, D., Huss, M., Dussailant, I., Brun, F., et al.: Accelerated global glacier mass loss in the early twenty-first century, *Nature*, 592, 726–731, 2021.
- 465 Huss, M. and Farinotti, D.: Distributed ice thickness and volume of all glaciers around the globe, *Journal of Geophysical Research: Earth Surface*, 117, 2012.
- Huss, M. and Hock, R.: Global-scale hydrological response to future glacier mass loss, *Nature Climate Change*, 8, 135–140, 2018.
- Immerzeel, W. W., Lutz, A. F., Andrade, M., Bahl, A., Biemans, H., Bolch, T., Hyde, S., Brumby, S., Davies, B., Elmore, A., et al.: Importance and vulnerability of the world’s water towers, *Nature*, 577, 364–369, 2020.





- 470 Joughin, I., Smith, B., Howat, I., and Scambos, T.: MEaSURES Multi-year Greenland Ice Sheet Velocity Mosaic, Version 1, <https://doi.org/10.5067/QUA5Q9SVMSJG>, 2016.
- Jouvet, G.: Inversion of a Stokes glacier flow model emulated by deep learning, *Journal of Glaciology*, 69, 13–26, 2023.
- Jouvet, G., Cordonnier, G., Kim, B., Lüthi, M., Vieli, A., and Aschwanden, A.: Deep learning speeds up ice flow modelling by several orders of magnitude, *Journal of Glaciology*, 68, 651–664, 2022.
- 475 Liu, Z., Koo, Y., and Rahnemoo, M.: Physics-Informed Machine Learning On Polar Ice: A Survey, arXiv preprint arXiv:2404.19536, 2024.
- Lundberg, S. M. and Lee, S.-I.: A unified approach to interpreting model predictions, *Advances in neural information processing systems*, 30, 2017.
- Martone, M., Rizzoli, P., Wecklich, C., González, C., Bueso-Bello, J.-L., Valdo, P., Schulze, D., Zink, M., Krieger, G., and Moreira, A.: The  
480 global forest/non-forest map from TanDEM-X interferometric SAR data, *Remote sensing of environment*, 205, 352–373, 2018.
- Masson-Delmotte, V., Zhai, P., Pirani, A., Connors, S. L., Péan, C., Berger, S., Caud, N., Chen, Y., Goldfarb, L., Gomis, M., et al.: Climate change 2021: the physical science basis, Contribution of working group I to the sixth assessment report of the intergovernmental panel on climate change, 2, 2391, 2021.
- Maussion, F., Rothenpieler, T., Dusch, M., Schmitt, P., Vlug, A., Schuster, L., Champollion, N., Li, F., Marzeion, B., Oberrauch, M., Eis,  
485 J., Fischer, A., Landmann, J., Jarosch, A., Iuzupaz, Hanus, S., Rounce, D., Castellani, M., Bartholomew, S. L., Minallah, S., Bowen-  
belongstonature, Merrill, C., Otto, D., Loibl, D., Rosa, G., Ultee, L., Thompson, S., Anton, U., and Gregor, P.: OGGM/oggm: v1.6.1, <https://doi.org/10.5281/zenodo.8287580>, 2023.
- Millan, R., Mouginot, J., Rabatel, A., and Morlighem, M.: Ice velocity and thickness of the world's glaciers, *Nature Geoscience*, 15, 124–129, 2022.
- 490 Morlighem, M.: MEaSURES BedMachine Antarctica, Version 3, <https://doi.org/10.5067/FPSU0V1MWUB6>, 2022a.
- Morlighem, M. e. a.: IceBridge BedMachine Greenland, Version 5, <https://doi.org/10.5067/GMEVBWFLWA7X>, 2022b.
- Mouginot, J., Rignot, E., and Scheuchl, B.: MEaSURES Phase-Based Antarctica Ice Velocity Map, Version 1, <https://doi.org/10.5067/PZ3NJ5RXHR10>, 2019.
- Muñoz-Sabater, J., Dutra, E., Agustí-Panareda, A., Albergel, C., Arduini, G., Balsamo, G., Boussetta, S., Choulga, M., Harrigan, S., Hers-  
495 bach, H., et al.: ERA5-Land: A state-of-the-art global reanalysis dataset for land applications, *Earth system science data*, 13, 4349–4383, 2021.
- Noël, B., van de Berg, W. J., van Wessem, J. M., van Meijgaard, E., van As, D., Lenaerts, J. T. M., Lhermitte, S., Kuipers Munneke, P., Smeets, C. J. P. P., van Ulf, L. H., van de Wal, R. S. W., and van den Broeke, M. R.: Modelling the climate and surface mass balance of polar ice sheets using RACMO2 – Part 1: Greenland (1958–2016), *The Cryosphere*, 12, 811–831, <https://doi.org/10.5194/tc-12-811-2018>,  
500 2018.
- Noël, B. and van Kampenhout, L.: Downscaled 1 km RACMO2 data used in CESM2 Greenland SMB evaluation paper, <https://doi.org/10.5281/zenodo.3367211>, 2019.
- Noël, B., van Wessem, M., Wouters, B., Trusel, L., Lhermitte, S., and van den Broeke, M.: Data set: "Higher Antarctic ice sheet accumulation and surface melt rates revealed at 2 km resolution", <https://doi.org/10.5281/zenodo.10007855>, 2023.
- 505 Pfeffer, W. T., Arendt, A. A., Bliss, A., Bolch, T., Cogley, J. G., Gardner, A. S., Hagen, J.-O., Hock, R., Kaser, G., Kienholz, C., et al.: The Randolph Glacier Inventory: a globally complete inventory of glaciers, *Journal of glaciology*, 60, 537–552, 2014.



- Pörtner, H.-O., Roberts, D. C., Masson-Delmotte, V., Zhai, P., Tignor, M., Poloczanska, E., Weyer, N., et al.: The ocean and cryosphere in a changing climate, IPCC special report on the ocean and cryosphere in a changing climate, 1155, 2019.
- Prokhorenkova, L., Gusev, G., Vorobev, A., Dorogush, A. V., and Gulin, A.: CatBoost: unbiased boosting with categorical features, *Advances in neural information processing systems*, 31, 2018.
- 510 Rodell, M., Famiglietti, J. S., Wiese, D. N., Reager, J., Beaudoing, H. K., Landerer, F. W., and Lo, M.-H.: Emerging trends in global freshwater availability, *Nature*, 557, 651–659, 2018.
- Rounce, D. R., Hock, R., Maussion, F., Hugonnet, R., Kochtitzky, W., Huss, M., Berthier, E., Brinkerhoff, D., Compagno, L., Copland, L., et al.: Global glacier change in the 21st century: Every increase in temperature matters, *Science*, 379, 78–83, 2023.
- 515 Tober, B., Holt, J., Christoffersen, M., Truffer, M., Larsen, C., Brinkerhoff, D., and Mooneyham, S.: Comprehensive radar mapping of Malaspina Glacier (Sít’Tlein), Alaska—The world’s largest piedmont glacier—Reveals potential for instability, *Journal of Geophysical Research: Earth Surface*, 128, e2022JF006 898, 2023.
- Uroz, L. L., Yan, Y., Benoit, A., Rabatel, A., Giffard-Roisin, S., and Lin-Kwong-Chon, C.: Using Deep Learning for Glacier Thickness Estimation at a Regional Scale, *IEEE Geoscience and Remote Sensing Letters*, 2024.
- 520 Welty, E., Zemp, M., Navarro, F., Huss, M., Fürst, J. J., Gärtner-Roer, I., Landmann, J., Machguth, H., Naegeli, K., Andreassen, L. M., et al.: Worldwide version-controlled database of glacier thickness observations, *Earth System Science Data Discussions*, 2020, 1–27, 2020.
- Zemp, M., Huss, M., Thibert, E., Eckert, N., McNabb, R., Huber, J., Barandun, M., Machguth, H., Nussbaumer, S. U., Gärtner-Roer, I., et al.: Global glacier mass changes and their contributions to sea-level rise from 1961 to 2016, *Nature*, 568, 382–386, 2019.